Batteries & Supercaps

Research Article
doi.org/10.1002/batt.202400214

Chemistry Europe
European Chemical Societies Publishing

www.batteries-supercaps.org

Olivine $NaMn_{0.66}Fe_{0.34}PO_4$ as a Cathode Material for Advanced Sodium Ion Batteries

Tassadit Ouaneche,[a, b, c] Lorenzo Stievano,[a, c] Laure Monconduit,[a, c] Claude Guéry,[b] Moulay Tahar Sougrati,*[a, c] and Nadir Recham*[b, c]

Sodium-ion batteries continue to rise in the energy storage landscape, their increasing adoption being driven by factors such as cost-effectiveness and sustainability. As a consequence, there is a growing emphasis on the development of new electrode materials. Among these, olivine phosphates emerge as a promising family of cathode materials. However, viable synthesis routes are still lacking. In this study, cathode materials of olivine $NaMn_{1-x}Fe_xPO_4$ (x = 0.34 and 1) were prepared by directly sodiating $Mn_{1-x}Fe_xPO_4$ through a solid-state process at 300 °C. X-ray diffraction, Mössbauer spectroscopy and electrochemical measurements were employed to study their structural and electrochemical features. $NaMn_{0.66}Fe_{0.34}PO_4$ exhibits two pseudo-plateaus profile with an average potential of ~3.2 V vs. Na^+/Na^0 with a reversible capacity reaching 75 mAh/g at C/20 via a monophasic (de)intercalation mechanism. In parallel, the intermediate composition $Na_{0.5}Mn_{0.66}Fe_{0.34}PO_4$ could be prepared via the solid-state reaction of $NaMn_{0.66}Fe_{0.34}PO_4$ and $Mn_{0.66}Fe_{0.34}PO_4$. Such a solvent-free sodiation process not only provides a simplified preparation of NMFP, but also offers easy scalability compared to the more laborious electrochemical sodiation route, making it an interesting prospect for future industrialization. Finally, this research confirms that the olivine NMFP is indeed an attractive candidate as a cathode material for SIBs.

1. Introduction

In recent years, the quest for efficient and sustainable energy storage solutions has sparked significant interest in alternative battery technologies, with sodium-ion batteries (SIBs) emerging as promising contenders.[1] As the demand for electric batteries and grid energy storage continues to rise, nowadays, there is a considerable interest in SIBs due to their interesting properties (*i.e.*,, abundant and low-cost elements and raw materials) compared to conventional lithium-ion batteries.[2,3] Given the significant growing interest in SIBs, numerous companies have ventured into the sector as part of their business operations, among them are: CATL and HiNa Tech (China), Faradion (UK), Natron Energy (US) and Tiamat Energy (France).

In SIBs, the positive electrode is primarily composed of Na_xMO_2 layered oxides ($x \leq 1$ and M = transition metal ion(s)),[4] which offer benefits such as abundant elements and low molar masses, resulting in good specific capacity. However, as these materials exhibit a potential lower than 3 V *vs.* Na^+/Na^0, they are unstable in air due to their rapid oxidation in presence of moisture,[5,6,7] and they also cannot be formulated with water-based binders. Presently, one of the most promising positive electrode material is $Na_3V_2(PO_4)_2F_3$ (NVPF) due to its favorable potential and its rapid discharge rate.[8,9] Nevertheless, the presence of vanadium and fluorine in this material is undesirable, owing to their toxicity and the criticality of vanadium.[10] Other sodium-based promising cathode materials can be mentioned,[11] such as NASICON-type $Na_3V_2(PO_4)_3$ (NVP) and $Na_3V(PO_4)_2$ which are fluorine-free materials[12] compared to NVPF. NVP was found to possess great sodium storage capabilities under different voltage ranges, contributing to a theoretical capacity of 173 mAh/g at an average charge/discharge potential of 3.6 V for two e^- transfer per V.[12] One can also mention Na_2FePO_4F fluorophosphate material[13] which exhibits a potential of ~3.1 V *vs.* Na^+/Na^0.

Among the polyanionic-based cathode materials for SIBs, one promising candidate that has gained considerable attention in the last years is the olivine-type $NaFePO_4$ (NFP), analogous to olivine $LiFePO_4$ (LFP),[14] since it presents several advantages such as security and low cost, thermal and structural stability, eco-friendliness and a high theoretical capacity (154 mAh/g).[15] These favorable properties make it a serious contender for real applications and future industrialization.

$NaFePO_4$ exists as two distinct polymorphs, triphylite (*i.e.*, olivine) and maricite.[16] To date, the triphylite phase was not reported by direct synthesis at neither high nor moderate temperatures, which rather lead to the thermodynamically stable maricite allotrope. The latter, however, is characterized by a relatively tight structure, and is not attractive electrochemically owing to the lack of available pathways for Na^+ diffusion.[17,18]

[a] T. Ouaneche, L. Stievano, L. Monconduit, M. T. Sougrati
ICGM, Université Montpellier, CNRS, ENSCM, 34090, Montpellier, France
E-mail: moulay.tahar-sougrati@umontpellier.fr

[b] T. Ouaneche, C. Guéry, N. Recham
Laboratoire de Réactivité et de Chimie des Solides LRCS, CNRS UMR 7314, Université de Picardie Jules Verne, 80039, Amiens, France
E-mail: nadir.recham@u-picardie.fr

[c] T. Ouaneche, L. Stievano, L. Monconduit, M. T. Sougrati, N. Recham
Réseau sur le Stockage Electrochimique de l'Energie (RS2E), FR CNRS 3459, Amiens, France

Research Article
doi.org/10.1002/batt.202400214
Chemistry Europe
European Chemical Societies Publishing

Triphylite is then obtained by alternative routes, usually starting from $LiFePO_4$ and substituting Li^+ with Na^+ ions, or also through air oxidation of sacropside $Fe^{2+}{}_3(PO_4)_2$ phase.[19] Moreau et al.[14] synthesized olivine $NaFePO_4$ by electrochemical sodiation *vs.* sodium metal starting from olivine $FePO_4$ (FP) obtained by chemical delithiation of $LiFePO_4$ with NO_2BF_4. Casas-Cabanas *et al.*[20] studied the FP-NFP system by showing both chemical (using NaI) and electrochemical Na^+ insertion into FP. J. Lu, *et al.*,[21] later proposed a simple synthesis of olivine NFP by electrochemical as well as chemical oxidation/reduction methods, and by a solid-state method using NaI. All these articles confirm the promising electrochemical potential of olivine NFP of about 3 V *vs.* Na^+/Na^0. However, the overall electrochemical performance of the resulting NFP are moderate, especially for power applications that require cycling at high current rates.

To improve the energy density of NFP, the iron can be partially substituted by manganese to form the olivine $NaMn_{1-x}Fe_xPO_4$ (NMFP), which leads to an increase of the electrochemical potential. However, as in the case of NFP, no direct synthesis is reported for NMFP, and it is therefore necessary to start from a Li-based $LiMn_{1-x}Fe_xPO_4$ (LMFP) precursor and replace the Li^+ by Na^+ ions. In this work, the synthesis of olivine NMFP cathode is carried out by solid-state chemical sodiation of a previously desodiated LMFP precursor (MFP) with sodium iodide NaI at an intermediate temperature of 300 °C under argon. The obtained olivine NMFP was fully characterized by different techniques and tested electrochemically in half cell configuration *vs.* Na metal. In order to better understand the properties of the materials obtained via this original route, the synthesis and characterization of the olivine intermediate phase $Na_{0.5}Mn_{0.66}Fe_{0.34}PO_4$ as well as of the manganese-free NFP phase were also carried out. This solvent-free sodiation process does not only simplify the preparation of NMFP cathode materials, but can also be easily upscaled compared to the more laborious electrochemical sodiation routes, making it particularly interesting in the light of a potential future industrialization of this family of materials.

Experimental

Synthesis of $Na_xMn_{0.66}Fe_{0.34}PO_4$ (x = 1 and 0.5) and $NaFePO_4$

Olivine $NaMn_{0.66}Fe_{0.34}PO_4$ (NMFP) was obtained through a two-step reaction. First, pristine $LiMn_{0.66}Fe_{0.34}PO_4$ (S4R, France) was chemically delithiated using NO_2BF_4 (Sigma Aldrich, ≥ 95 %) in acetonitrile for 24 h, in air at ambient temperature. The obtained delithiated $Mn_{0.66}Fe_{0.34}PO_4$ (MFP) was sodiated by sodium iodide (NaI, Acros Organics, 99 %), used both as a reducing agent and as sodium source, via a solid-state process. After mixing stoichiometric amounts of the powders in a mortar, the mixture was heated at 300 °C for 10 h in a tubular furnace under argon flow. After the reaction, the sodiated NMFP was washed with water and ethanol, and finally dried at 60 °C under primary vacuum.

The intermediate olivine $Na_{0.5}Mn_{0.66}Fe_{0.34}PO_4$ phase was synthetized by mixing the sodiated NMFP and the totally delithiated MFP in a stoichiometric ratio of 50/50, and reacting them via a solid-state synthesis at 320 °C for 10 hours in a tubular furnace under argon. Schema 1 summarizes the synthesis steps of NMFP and $Na_{0.5}Mn_{0.66}Fe_{0.34}PO_4$.

Olivine NFP was synthetized using the method proposed by Lu.[21] Pristine $LiFePO_4$ (Targray) was fully chemically delithiated using an excess of iron(III) nitrate nonahydrate $Fe(NO_3)_3.9H_2O$ (Sigma Aldrich, ≥ 98 %) in aqueous solution for 12 h. The obtained delithiated olivine $FePO_4$ (FP) was sodiated by sodium iodide NaI (Acros Organics, 99 %) at 300 °C for 10 h under argon atmosphere, and finally processed as in the case of NMFP (*vide supra*).

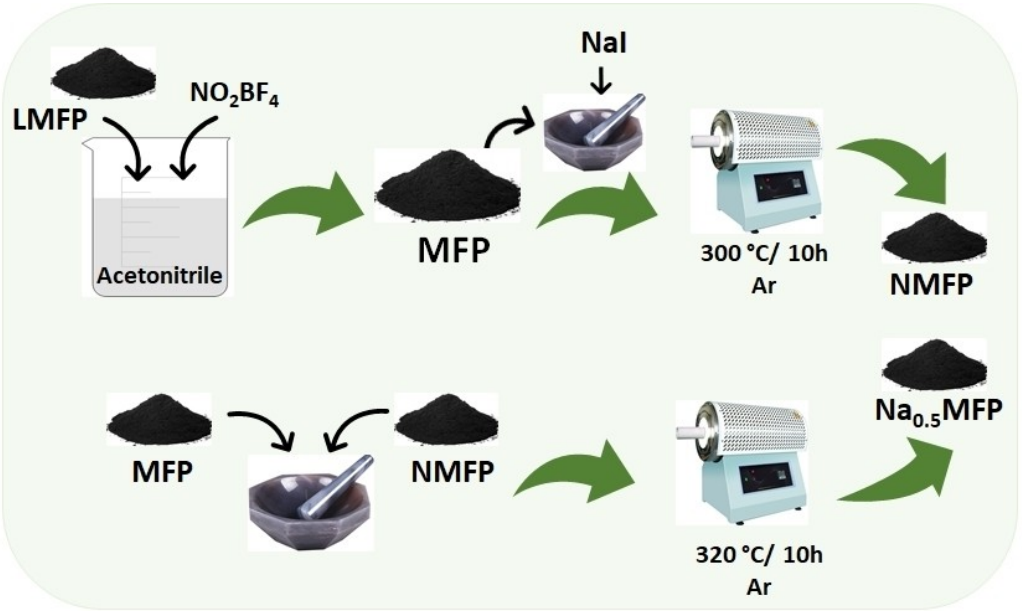

Scheme 1. Simplified schema of the solid-state synthesis of $NaMn_{0.66}Fe_{0.34}PO_4$ and $Na_{0.5}Mn_{0.66}Fe_{0.34}PO_4$.

Research Article
doi.org/10.1002/batt.202400214
Chemistry Europe
European Chemical Societies Publishing

Physico-Chemical Characterization

X-ray diffraction (XRD) measurements were carried out using a Bruker D8 Advance powder diffractometer equipped with the Cu K_α radiation (λ $K_{\alpha1}$ = 1,54056 Å and λ $K_{\alpha2}$ = 1,54439 Å) and with a Lynkeye detector operating at 40 kV and 40 mA. The patterns were collected between $2\Theta = 10^\circ$ and 60° with a step of 0.074. The powder XRD patterns were fitted using full Rietveld refinement as implemented in the FULLPROF program.

Transmission ^{57}Fe Mössbauer spectra were recorded at room temperature in the constant acceleration mode with a ^{57}Co:Rh source. The Mössbauer absorbers were prepared with 20–50 mg/cm^2 of cathode materials. The isomer shifts are referred to α-Fe metal at room temperature and the velocity scale was chosen between +/−4 mm/s and the acquisition time between 24–36 hours.

The powder morphology and chemical composition were examined by scanning electron microscopy (SEM) using a FEI Quanta 200-FEG coupled with energy dispersive X-ray spectroscopy (EDX).

Electrochemical Characterization

NMFP and NFP-based electrodes were prepared by tape casting of a slurry prepared by mixing the active material with C45 carbon black conductive additive and polyvinylidene fluoride (PVDF) as polymer binder in the mass ratio of 70:20:10 in N-Methyl-2-pyrrolidone (NMP). After stirring for 2 hours to achieve a homogeneous mixture, the slurry was coated on a 22 μm thick aluminum current collector by doctor blading and dried overnight under vacuum at 100 °C.

The standard electrochemical measurements in galvanostatic mode were performed in half-cell configuration *vs.* Na metal in Swagelok™-type cells, which were assembled inside an argon-filled glove box. The electrodes were separated by a Whatman® glass fibre soaked with a 1 M $NaPF_6$ dissolved in EC/DMC. The cells were evaluated in the voltage windows of 2.0–4.3 V at a current rate of C/50 and 2–4 V at C/200, for C/NMFP and C/NFP respectively.

The electrochemical performance of NMFP was evaluated by the galvanostatic intermittent titration technique (GITT) during charge and discharge using a specific *in situ* cell[22] with 25 mg of C/NMFP powder mixture (hand mixing) in the same configuration of that described above for the other electrochemical tests. Several sequences of 2 hours under oxidation/reduction current corresponding to a total charge of 0.1 Na^+ eq. per mole of NMFP were followed by relaxation times of 1 hour, when XRD patterns were measured in order to study the evolution of the structure of NMFP during charge and discharge.

2. Results and Discussion

Figure 1 shows the refinement of the XRD patterns of pristine LMFP, delithiated MFP and sodiated NMFP as well as their respective Mössbauer spectra. The XRD patterns of commercial LMFP (Figure 1a) and chemically delithiated MFP (Figure 1c) can both be indexed in the Pnma space group with cell parameters a = 10.396(1) Å, b = 6.060(1) Å, c = 4.722(1) Å and a = 9.702(1) Å, b = 5.857(1) Å, c = 4.777(1) Å for LMFP and MFP, respectively, confirming a total delithiation of LMFP.[23] Moreover, the XRD pattern of the sodiated phase (Figure 1e) shows the complete disappearance of the peaks of MFP and the presence of a single olivine phase corresponding to NMFP, with lattice parameters a = 10.479(1) Å, b = 6.280(1) Å and c = 4.970(1) Å. The volume of the sodiated phase is 327 Å^3, very close to that reported in the literature for $NaMn_{0.5}Fe_{0.5}PO_4$.[24]

The local environment of the iron centres was investigated by Mössbauer spectroscopy. Figure 1b shows the spectrum of pristine LMFP, which is perfectly fitted with a major doublet with an isomer shift and a quadrupole splitting of 1.22 and 2.96 mm/s, respectively, typical of octahedrally coordinated high spin Fe^{2+} and counting for about 97.5 % of the total resonance area (Table 1). The remaining 2.5 % of the resonance area corresponds to a minor component attributed to amorphous Fe_xP, a typical impurity usually found in commercial LMFP that is not altered by chemical delithiation nor by the further sodiation. The spectrum of MFP shown in Figure 1d confirms the total delithiation of LMFP, as it exhibits the presence of only Fe^{3+}, typical of olivine MFP with an isomer shift and a quadrupole splitting of 0.42 and 1.66 mm/s, respectively. Finally, the spectrum of NMFP in Figure 1f could be fitted using a dominant quadrupole doublet representing octahedrally coordinated high spin Fe^{2+} with an isomer shift of 1.23 mm/s and a quadrupole splitting of 2.76 mm/s.

Both the refined cell parameters and the Mössbauer spectroscopy results confirm that this solid-state process allows the complete sodiation of MFP to form olivine NMFP, reducing Fe^{3+} to Fe^{2+}. The oxidation of divalent iron occurring at a lower potential than that of manganese, from these results one can also infer that all Mn^{3+} was also reduced to Mn^{2+}. These reductions are accompanied by Na^+ insertion in the structure, according to the reaction (1):

$$Mn_{0.66}Fe_{0.34}PO_4 + NaI \rightarrow NaMn_{0.66}Fe_{0.34}PO_4 + {}^1/_2\ I_2 \quad (1)$$

The morphology of the particles of sodiated NMFP was verified by SEM coupled with EDX. The SEM image in Figure 2a shows the presence of individual secondary particles (agglom-

Table 1. Mössbauer hyperfine parameters of: $FePO_4$, $NaFePO_4$, $LiMn_{0.66}Fe_{0.34}PO_4$, $Mn_{0.66}Fe_{0.34}PO_4$ and $NaMn_{0.66}Fe_{0.34}PO_4$. IS, QS, LW and Abs are respectively the isomer shift, the quadrupole splitting, the linewidth and the relative absorption areas.

Samples	IS, mm/s	QS, mm/s	LW, mm/s	Abs, %	Attribution
$LiMn_{0.66}Fe_{0.34}PO_4$ (Figure 1b)	1.22	2.96	0.25	97.5	Fe^{2+} (LMFP)
	0.46	0.54	0.33	2.5	Fe^{3+}
$Mn_{0.66}Fe_{0.34}PO_4$ (Figure 1d)	0.42	1.66	0.33	97	Fe^{3+} (MFP)
	0.46	0.54	0.33	3	Fe^{3+}
$NaMn_{0.66}Fe_{0.34}PO_4$ (Figure 1f)	1.23	2.76	0.26	97.5	Fe^{2+} (NMFP)
	0.46	0.54	0.33	2.5	Fe^{3+}
$FePO_4$ (Figure 6b)	0.44	1.53	0.26	95	Fe^{3+} (FP)
	0.53	0.69	0.31	5	Fe^{3+}
$NaFePO_4$ (Figure 6c)	1.22	2.74	0.26	95	Fe^{2+} (NFP)
	0.53	0.69	0.31	5	Fe^{3+}

Research Article
doi.org/10.1002/batt.202400214
Chemistry Europe
European Chemical Societies Publishing

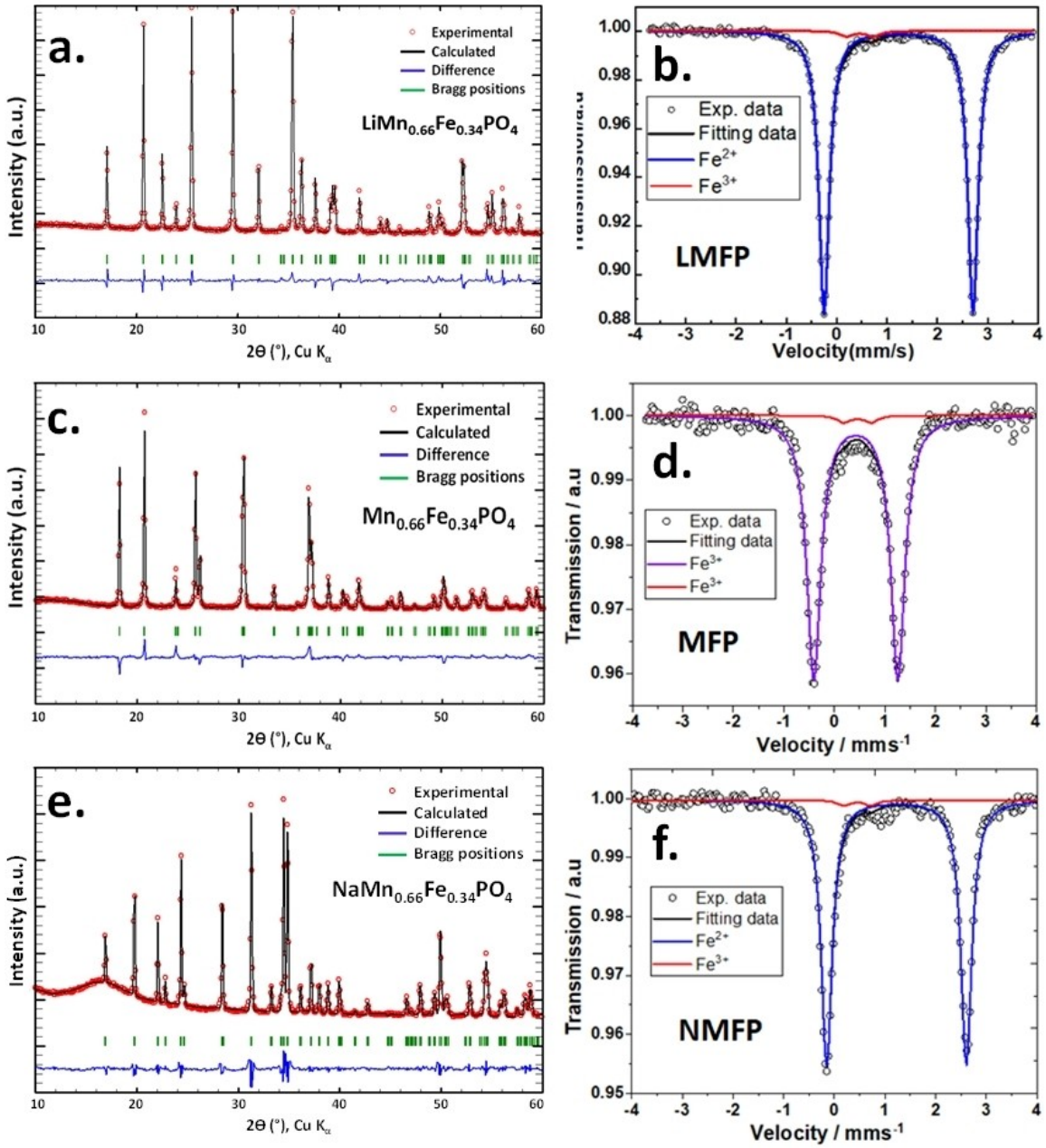

Figure 1. Refined X-ray diffraction patterns of **a)**. pristine $LiMn_{0.66}Fe_{0.34}PO_4$, **c)**. delithiated $Mn_{0.66}Fe_{0.34}PO_4$ and **e**. sodiated $NaMn_{0.66}Fe_{0.34}PO_4$ and their corresponding Mössbauer spectra **b**–**f)**, respectively.

erates of primary particles), with a size distribution between 50 and 200 nm. In parallel, the EDX mapping in Figure 2b shows the homogeneous distribution of the probed elements with an average Na/Mn/Fe/P ratio of about 30/20/17/33 (±5%). This result once again confirms the total sodiation of NMFP.

The electrochemical performance of sodiated NMFP (inset in Figure 3) studied in galvanostatic mode at C/50 shows that the material is electrochemically active *vs.* Na metal with an equilibrium potential of about ~3.2 V. Moreover, the S-shaped curve in the first charge shows two pseudo plateaus: a first one at ~3.0–3.5 V of about 50 mAh/g (~0.3 Na) corresponding to the oxidation of Fe^{2+} to Fe^{3+}, and a second one at ~3.7 V of about 55 mAh/g (~0.35 Na) related to the Mn^{3+}/Mn^{2+} redox couple.

In discharge, a capacity of about 85 mAh/g is recovered over a single sloping part, which does not allow the distinction of the processes corresponding to the reduction of Fe and Mn. A stable reversible charge/discharge capacity of 60–75 mAh/g is observed along the following 35 cycles at C/20 (Figure 3), showing an interesting performance that however needs to be improved. In fact, the obtained low stable coulombic efficiency especially for the first cycle might be due to different reasons such as: i) the non-optimization of the electrode formulation, ii) a very low Mn solubility during cycling, iii) since the same and

Research Article
doi.org/10.1002/batt.202400214
Chemistry Europe
European Chemical Societies Publishing

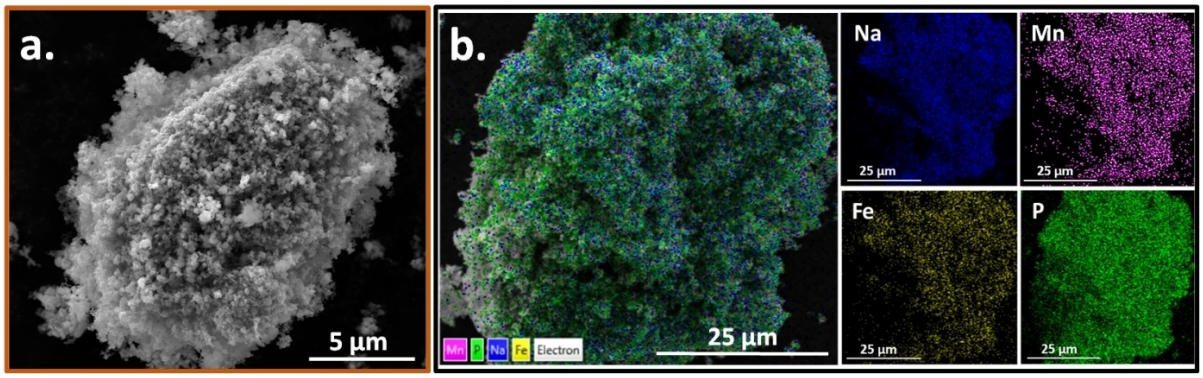

Figure 2. a). SEM Secondary electron (SE) image and **b)**. EDX elemental identification of Na, Mn, Fe and P of NMFP.

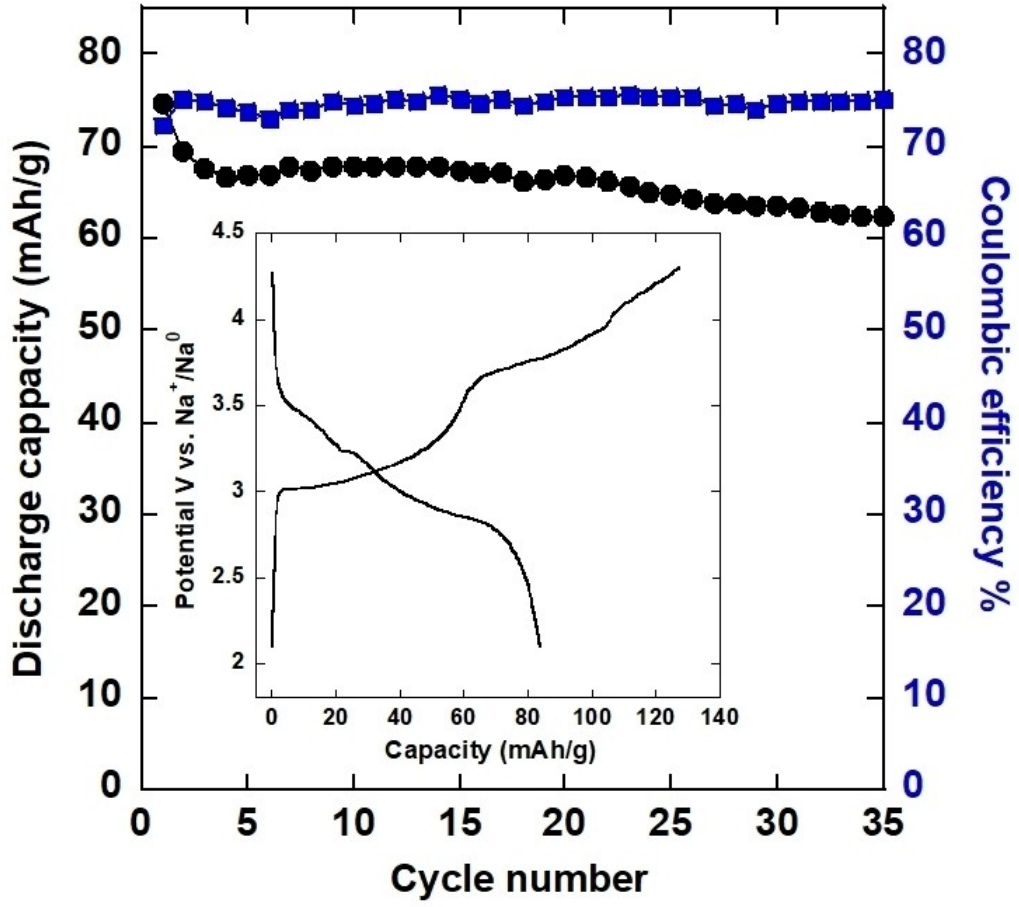

Figure 3. Cyclability in discharge of $NaMn_{0.66}Fe_{0.34}PO_4$ vs. Na^+/Na^0 for 35 cycles at C/20 with its coulombic efficiency. And its inserted charge-discharge galvanostatic curves corresponding to the first cycle at C/50.

stable CE and the discharge capacity are observed during the 35 cycles (~75% CE), some electrolyte decomposition may be the major reason of this low observed CE. Finally, the absence of well-defined plateaus, as observed for LMFP in lithium batteries, suggests the possible occurring of a monophasic (de)insertion mechanism. To confirm this hypothesis, *in situ* XRD was coupled to GITT to depict the phase evolution during charge and discharge, with patterns sequentially measured during the relaxation steps after the reaction of 0.1 eq. Na^+ per mole of NMFP.

The results of the GITT analysis confirm those previous obtained by galvanostatic cycling. During the charge process, two regions are observed, corresponding to the oxidation of Fe and Mn centers. It is noteworthy that the polarization observed by GITT is higher for the Mn plateau at higher potential than for the Fe one. In discharge, an S-shaped profile without any well-defined plateau is observed starting from higher potentials

Research Article
doi.org/10.1002/batt.202400214
Chemistry Europe
European Chemical Societies Publishing

than those observed during the previous charge. It is worth noting, however, that only 0.7 Na^+ could be disinserted during the GITT charge process at C/20, probably due to the non-optimized formulation of the powder electrode.

The XRD patterns measured in the 2θ range 28°–38° (Figure 4), during charge and discharge show a monophasic mechanism with the presence of only a single olivine-type phase with varying peak positions. During the charge, two main regions can be observed: from 1 to 0.6 Na^+ eq., a shift of the peaks to higher 2θ (for example the (301) peak) is observed, while from 0.5 to 0.3 Na^+ eq. a shift to lower angles is observed instead. The first region is characterized by an increase of the potential up to 3.8 V, which should correspond to the oxidation of Fe^{2+}, whereas the second one corresponds to a potential between 3.8 V and 4 V, which might correspond to the oxidation of Mn^{2+}.

Only the first of these two phenomena is observed during the discharge, with first a shift of 2θ to lower angles up to 0.4 Na^+ eq. This process is followed by a region where the no shift of the XRD peaks can be detected in spite of the continuation of the electrochemical reaction. These differences between charge and discharge may explain the different electrochemical profiles between the two processes. In conclusion, olivine NMFP seems to evolve during both charge and discharge through a single solid solution domain. It is also worth mentioning that a larger shift of the XRD patterns was observed during the charge than during the discharge, and that the pattern of the pristine state could not be recovered during the discharge.

The monophasic (de)insertion mechanism of NMFP shown by *in situ* XRD suggested the possibility of synthesizing intermediate $Na_xMn_{0.66}Fe_{0.34}PO_4$ compositions by simple chemical sodiation using NaI, by electrochemical sodiation or even directly by studying the reactivity of NMFP/MFP mixtures via a solid-state reaction, as it was done by Delacourt *et al.* to obtain olivine $Li_{0.5}FePO_4$.[25] Figure 5 shows the XRD patterns of three phases: NMFP, MFP and $Na_{0.5}Mn_{0.66}Fe_{0.34}PO_4$ synthesized by solid-state reaction of the first two. The XRD pattern of $Na_{0.5}Mn_{0.66}Fe_{0.34}PO_4$ matches well that of the intermediate phase obtained after the electrochemical extraction of 0.5 Na^+ eq. from NMFP (*vide supra*, Figure 4). This result shows that such a process can be in principle applied to synthesize all possible

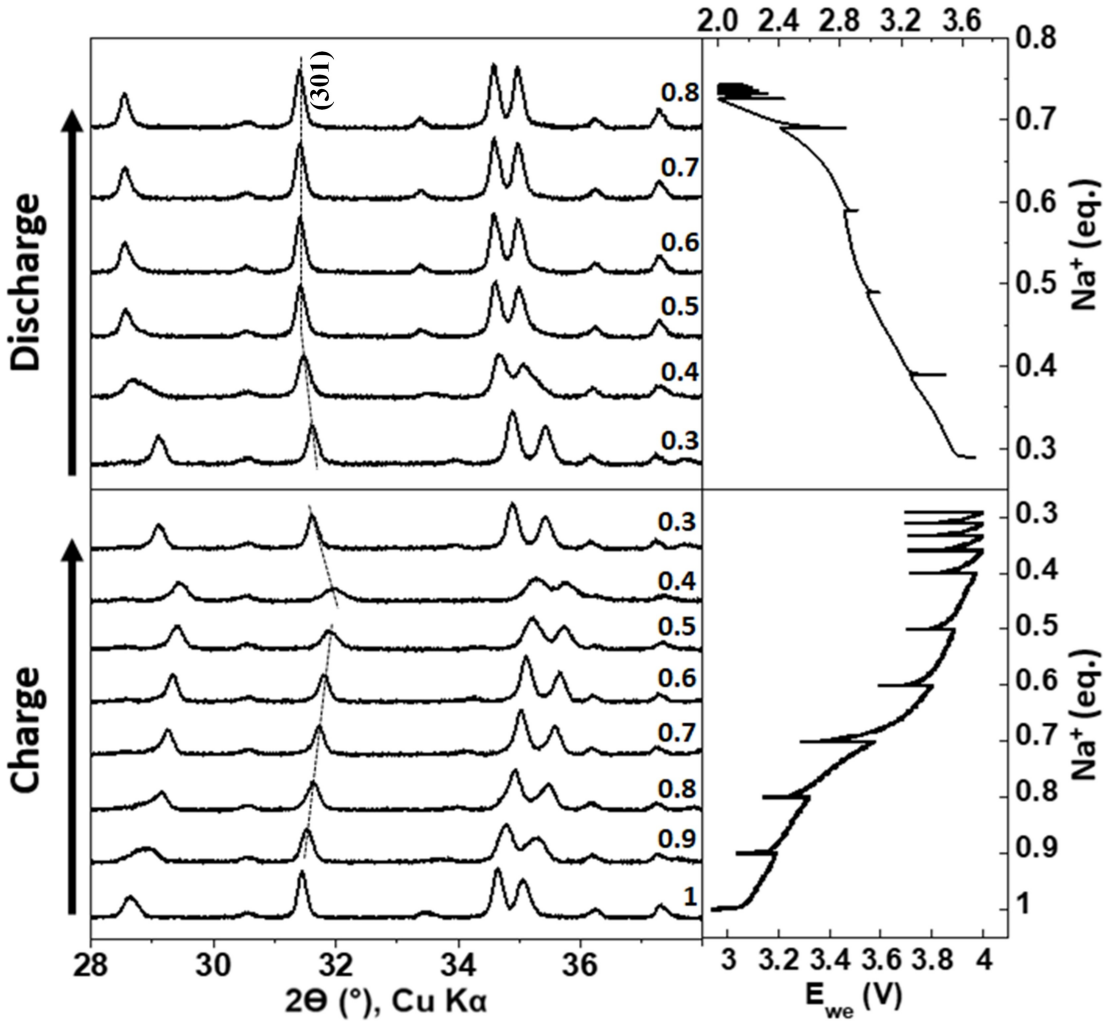

Figure 4. In-situ X-ray diffractograms of $NaMn_{0.66}Fe_{0.34}PO_4$ recorded during the electrochemical process in GITT mode at C/20 vs. Na^+/Na^0 at room temperature.

Research Article
doi.org/10.1002/batt.202400214
Chemistry Europe
European Chemical Societies Publishing

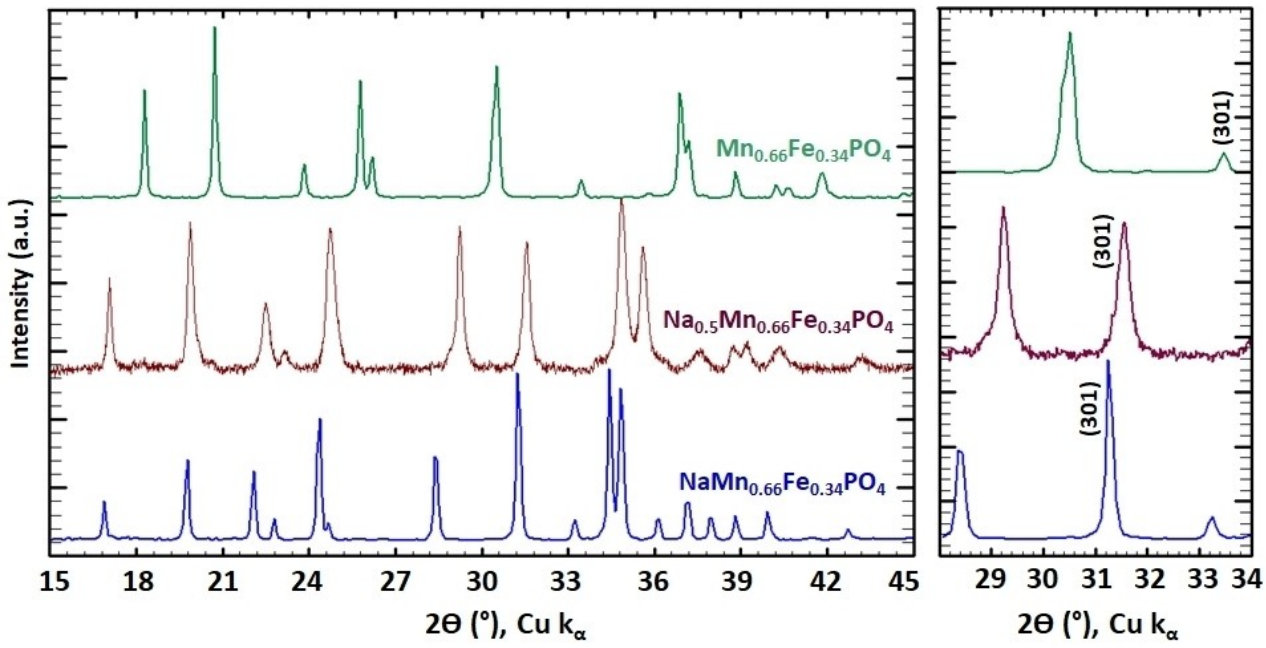

Figure 5. X-ray diffractograms of $NaMn_{0.66}Fe_{0.34}PO_4$, $Na_{0.5}Mn_{0.66}Fe_{0.34}PO_4$ (recorded after a mix of 0.5NMFP and 0.5MFP), and $Mn_{0.66}Fe_{0.34}PO_4$.

compositions of the $Na_xMn_{0.66}Fe_{0.34}PO_4$ family, by the study of NMFP/MFP binary diagram.

It is interesting to stress that, in the different research works on NFP cathodes for SIBs, its sodiation state could not always be confirmed by specific analytical methods. In this perspective, Mössbauer spectroscopy may be the method of choice to confirm the sodiation state via the study of the physico-chemical state of the iron centers. To prove the efficiency of this approach, the study of an olivine NFP prepared from a commercial LFP powder using the method proposed by J. Lu, *et al.*,[21] was studied in parallel by both XRD and Mössbauer spectroscopy.

Figure 6a shows the XRD patterns of both delithiated $FePO_4$ (FP) and chemically sodiated NFP. Sodium insertion via the proposed solvent free sodiation process leads to the total disappearance of FP, and the formation of pure olivine NFP, corresponding to an increase of the cell parameters to the following values determined by Rietveld refinement: Pnma space group, a = 10.390(1) Å, b = 6.216(1) Å and c = 4.942(1) Å, which match well with those reported for NFP in the literature.[14]

The Fe speciation of the two materials FP and NFP was followed by Mössbauer spectroscopy. Figure 6b shows the Mössbauer spectrum of delithiated FP, which exhibits only the quadrupole doublet typical of Fe^{3+} in FP. A second component representing very minor amounts of amorphous Fe_xP species commonly found in commercial LFP, is also detected.[26] Such a pollution, not observed by XRD because of its amorphous nature, is usually formed during the synthesis of LFP at high temperatures under reducing conditions.[27]

The Mössbauer spectrum of sodiated NFP (Figure 6c), on the other hand, confirms the full reduction of iron, as only the typical quadrupole doublet of high spin Fe^{2+}, with an IS of 1.22 mm/s accounting for 95% of the total resonance area (cf. Table 1) is visible. The remaining 5% of the resonance area is represented by the minor doublet of amorphous Fe_xP species, already contained in pristine LFP. This reduction is accompanied by the full insertion of sodium in the FP structure following reaction (2).

$$FePO_4 + NaI \rightarrow NaFePO_4 + {}^1/_2\ I_2 \quad (2)$$

The electrochemical signature of the obtained NFP, shown in inset-Figure 6d, perfectly reproduces those reported in the literature.[28] A reversible capacity of about ~120 mAh/g is obtained, corresponding to the (de)insertion of ~0.8 Na eq. per mole of NFP at C/200, which also reproduces the typical values of the literature.[21] Additionally, Figure 6d shows a stable low discharge capacity of ~55 mAh/g at a current rate of C/20 and a coulombic efficiency $< 80\%$.

3. Conclusions

The synthesis of various members of the olivine family, specifically $Na_xMn_{0.66}Fe_{0.34}PO_4$ (x = 0, 0.5, 1), was obtained by a straightforward solid-state approach. $NaMn_{0.66}Fe_{0.34}PO_4$ was synthesized through solid-state chemical sodiation with NaI at 300 °C, while $Na_{0.5}Mn_{0.66}Fe_{0.34}PO_4$ was produced via a simple solid-state reaction at 320 °C using a 1/1 ratio of the two end-members (MFP and NMFP). Characterization techniques, including *in situ* XRD, confirmed a monophasic (de)insertion mechanism of Na^+ in NMFP with a S-shaped electrochemical profile, which could be a very useful feature for the facile determination of the charge state in a practical battery application. NMFP exhibits a reversible discharge capacity of approximately

Research Article
doi.org/10.1002/batt.202400214
Chemistry Europe
European Chemical Societies Publishing

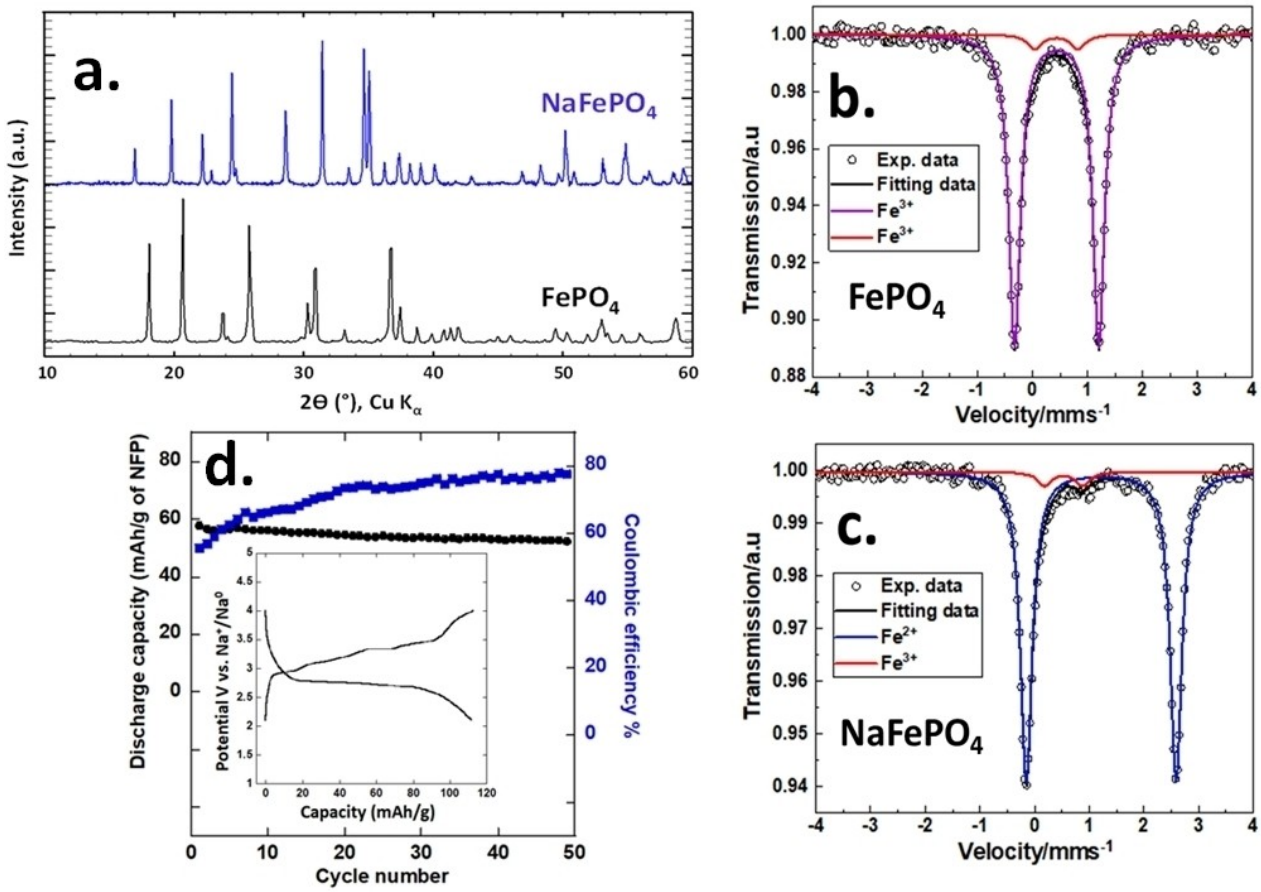

Figure 6. a). X-ray diffraction patterns of delithiated $FePO_4$ and sodiated $NaFePO_4$, Mössbauer spectra of **b**). $FePO_4$ and **c**). $NaFePO_4$. And **d**). discharge capacity of $NaFePO_4$ *vs.* Na^+/Na^0 for 50 cycles at a current rate of C/20 with its coulombic efficiency, with its inserted charge-discharge galvanostatic curves corresponding to the first cycle at C/200 at room temperature.

~75 mAh/g. This moderate reversible capacity indicates a more complex reversible (de)insertion mechanism of Na^+ which can be attributed to the lower Na^+ diffusion in the olivine structure. Further experimental effort is needed to support these findings as well as to optimize electrode preparation, in order to gain a deeper understanding of the reaction mechanism and to push such materials to the best of their performance.

Acknowledgements

The authors gratefully acknowledge financial support from the French National Research Agency (project Labex STORE-EX, ANR-10-LABX-76-01). We also thank Dr. Arash Jamali for its precious help in recording the SEM images.

Conflict of Interests

The authors declare no conflict of interest.

Data Availability Statement

Research data are not shared.

Keywords: Sodium-ion battery · NFP · NMFP · chemical sodiation · cathode material · olivine

[1] T. Hosaka, K. Kubota, A. S. Hameed, S. Komaba, *Chem. Rev.* **2020**, *120*, 6358–6466.
[2] M. Sawicki, L. L. Shaw, *RSC Adv.* **2015**, *5*, 53129–53154.
[3] S. Kim, D. Seo, X. Ma, G. Ceder, K. Kang, *Adv. Energy Mater.* **2012**, *2*, 710–721.
[4] S. Mariyappan, Q. Wang, J. M. Tarascon, *J. Electrochem. Soc.* **2018**, *165*, A3714–A3722.
[5] S. Mariyappan, Q. Wang, J. M. Tarascon, *J. Electrochem. Soc.* **2018**, *165*, A3714–A3722.
[6] J. Deng, W. Luo, S. Chou, H. Liu, S. Dou, *Adv. Energy Mater.* **2018**, *8*, 1–17.
[7] K. Kubota, S. Kumakura, Y. Yoda, K. Kuroki, S. Komaba, *Adv. Energy Mater.* **2018**, *8*, 1–30.
[8] G. Yan, et al., *Nat. Commun.* **2019**, *10*, 585.
[9] T. Broux, et al., *Small Methods* **2019**, *3*, 1–12.
[10] G. J. Simandl, S. Paradis, *Appl. Earth Sci.* **2022**, *131*, 218–236.
[11] T. Jin, et al., *Chem. Soc. Rev.* **2020**, *49*, 2342–2377.
[12] V. M. Kovrugin, R. David, J.-N. Chotard, N. Recham, C. A. Masquelier, *Inorg. Chem.* **2018**, *57*, 8760–8768.
[13] N. Recham, et al., *J. Electrochem. Soc.* **2009**, *156*, A993.

Research Article
doi.org/10.1002/batt.202400214

[14] P. Moreau, D. Guyomard, J. Gaubicher, F. Boucher, *Chem. Mater.* **2010**, *22*, 4126–4128.
[15] Y. Zhu, Y. Xu, Y. Liu, C. Luo, C. Wang, *Nanoscale* **2013**, *5*, 780–787.
[16] S. N. Yadav, S. J. Rajoba, R. S. Kalubarme, V. G. Parale, L. D. Jadhav, *Chinese J. Phys.* **2021**, *69*, 134–142.
[17] M. Avdeev, et al., *Inorg. Chem.* **2013**, *52*, 8685–8693.
[18] S.-M. Oh, S.-T. Myung, J. Hassoun, B. Scrosati, Y.-K. Sun, *Electrochem. commun.* **2012**, *22*, 149–152.
[19] C. Crouzet, et al., *Solid State Sci.* **2016**, *62*, 29–33.
[20] M. Casas-Cabanas, et al., *J. Mater. Chem.* **2012**, *22*, 17421–17423.
[21] J. Lu, S. C. Chung, S. I. Nishimura, A. Yamada, *Chem. Mater.* **2013**, *25*, 4557–4565.
[22] J. B. Leriche, et al., *J. Electrochem. Soc.* **2010**, *157*, A606.
[23] M. Kope, et al., *J. Power Sources* **2009**, *189*, 1154–1163.
[24] K. T. Lee, T. N. Ramesh, F. Nan, G. Botton, L. F. Nazar, *Chem. Mater.* **2011**, *23*, 3593–3600.
[25] C. Delacourt, P. Poizot, J.-M. Tarascon, C. Masquelier, *Nat. Mater.* **2005**, *4*, 254–260.
[26] M. Konarova, I. Taniguchi, *J. Power Sources* **2009**, *194*, 1029–1035.
[27] T. Ouaneche, et al., *J. Power Sources* **2023**, *579*, 233248.
[28] C. Berlanga, et al., *ACS Sustain. Chem. Eng.* **2020**, *8*, 725–730.

Manuscript received: March 29, 2024
Revised manuscript received: May 17, 2024
Version of record online: June 28, 2024